



OPEN

Automated segmentation of the mandibular canal and its anterior loop by deep learning

Nicolly Oliveira-Santos^{1,2}, Reinhilde Jacobs^{1,3✉}, Fernando Fortes Picoli^{1,4}, Pierre Lahoud¹, Liselot Niclaes¹ & Francisco Carlos Groppo^{1,5}

Accurate mandibular canal (MC) detection is crucial to avoid nerve injury during surgical procedures. Moreover, the anatomic complexity of the interforaminal region requires a precise delineation of anatomical variations such as the anterior loop (AL). Therefore, CBCT-based presurgical planning is recommended, even though anatomical variations and lack of MC cortication make canal delineation challenging. To overcome these limitations, artificial intelligence (AI) may aid presurgical MC delineation. In the present study, we aim to train and validate an AI-driven tool capable of performing accurate segmentation of the MC even in the presence of anatomical variation such as AL. Results achieved high accuracy metrics, with 0.997 of global accuracy for both MC with and without AL. The anterior and middle sections of the MC, where most surgical interventions are performed, presented the most accurate segmentation compared to the posterior section. The AI-driven tool provided accurate segmentation of the mandibular canal, even in the presence of anatomical variation such as an anterior loop. Thus, the presently validated dedicated AI tool may aid clinicians in automating the segmentation of neurovascular canals and their anatomical variations. It may significantly contribute to presurgical planning for dental implant placement, especially in the interforaminal region.

The mandibular canal (MC) extends bilaterally from the mandibular foramen to the mental foramen carrying the inferior alveolar nerve (IAN) and blood vessels, innervating and vascularizing the ipsilateral lower teeth and periodontal tissues directly or through its branches. The MC crosses the mental foramen towards the interforaminal region, where it separates into the mental canal and the incisive canal¹. While the incisive canal emerges anteriorly, the mental canal curves upward, backward, and lateral to reach the mental foramen². The mental foramen location varies from below the mandibular canine to the first molar but is commonly situated below the mandibular second premolar^{3,4}. Occasionally, the mental canal curving occurs more anteriorly, then looping backward and upward, forming the so-called anterior loop (AL) of the IAN^{5,6}. Anatomical variations of the MC, such as AL, must be detected to avoid nerve injury during oral and maxillofacial surgical procedures, such as genioplasty and dental implant placement⁶⁻¹¹.

The reported prevalence of AL ranges widely from 0 to 94% depending on geographical variations, the applied definition, and related assessment methods^{3,5,10,12-14}, thus hampering comparative studies. While some studies define AL as an extension without minimal distance from the mental foramen¹⁵, other authors suggest that this anterior extension must be at least 1 mm or 2 mm^{3,6}. Also, there seems to be a relationship between the location of the mental foramen and the presence of the AL. The AL is often detected when the mental foramen is located apically to the second premolar¹². Clinicians may be assisted by artificial intelligence (AI) to allow for automated visualization of the entire mandibular canal trajectory. Nowadays, AI tools are increasingly introduced for detecting and segmenting anatomical structures and pathology¹⁶⁻¹⁸. Considering the importance of accurately localizing the MC anatomy, deep learning (DL) techniques were developed to automatically detect and segment the MC using cone-beam computed tomography (CBCT) images. These canal segmentation tools allow highly accurate results, highlighting the importance of DL to efficient treatment planning, especially to implant placement¹⁹⁻²¹. However, there is still a need to generalize the DL tools to enable the detection and segmentation of anatomical MC variations. It undoubtedly also applies to the automated detection and segmentation of AL. Therefore, the

¹OMFS IMPATH Research Group, Department of Imaging and Pathology, KU Leuven and University Hospitals Leuven, UZ Campus St Rafael, Leuven, Belgium. ²Department of Oral Diagnosis, Piracicaba Dental School, University of Campinas (UNICAMP), Piracicaba, São Paulo, Brazil. ³Department of Dental Medicine, Karolinska Institutet, Stockholm, Sweden. ⁴Department of Stomatology and Oral Radiology, Dental School, Federal University of Goiás, Goiânia, Goiás, Brazil. ⁵Department of Biosciences, Piracicaba Dental School, University of Campinas (UNICAMP), Piracicaba, São Paulo, Brazil. ✉email: reinhilde.jacobs@ki.se

aim of the present study was to train and validate a dedicated cloud-based AI-driven tool to allow accurate and timely segmentation of the MC and its AL on CBCT scans.

Results

Table 1 shows the mean and standard deviation of the IoU, DSC, HD, Precision, Recall, and Accuracy measures of the testing dataset. No significant difference in the metrics between the segmentation of the MC with and without AL was noted ($p > 0.05$). Notwithstanding, the mean of Recall and Precision metrics were 0.965 and 0.672, respectively, showing that there was more under-segmentation, meanwhile providing a global accuracy of 0.997.

The median time from AI-driven segmentation was 22.5 s, whereas the median time from refined AI segmentation was 156 s. The time for refined AI segmentation in the posterior section was longer than for the anterior and middle sections ($p \leq 0.05$). There were no significant differences in the time needed to refine AI segmentation of anterior and middle sections, regardless of the presence of AL ($p > 0.05$) (Fig. 1). It implies that in the mental foramen region, the presence of the AL did not compromise AI segmentation. The anterior and middle sections also presented the most accurate AI segmentation.

Discussion

The correct detection of the MC is crucial to avoid per-operative nerve injury. However, in cases of anatomical variations of the MC, such as AL, correct identification becomes a challenge, even for oral radiologists and surgeons. In such cases, the detection by AI may overcome the limitation of the human eyes. In our study, besides the MC segmentation achieving much better metrics than previous AI-based segmentation of the MC on CBCT images^{19–21}, the present study is the first to show a unique AI network detecting anatomical variations such as the AL. On top of that, the currently described approach is based on Lahoud et al.²¹ being the only approach to detect yet fully, timely, and accurately segment the neurovascular canal along its course in the mandible.

Due to the anatomic complexity of the mental foramen region, such as the presence of AL, many authors highlighted the importance of the preoperative diagnosis with CBCT images during surgical planning near the mental foramen^{3,6,9,14,22}. Even though there is high variability in the prevalence, length, gender, and side distribution of AL in various populations considering a high heterogeneity of reported methodologies to evaluate AL¹². Because of this variability, some authors stated it is difficult to recommend reliable fixed safety margins for surgical procedures such as implant placement^{22,23}. Therefore, following the methodology of Krishnan et al.³, we only considered AL if it was bigger than 1 mm, also considering that a more considerable variability from the regular course of the MC would bring a more significant challenge for the AI network to recognize. Notwithstanding, there was no difference in the AI-driven segmentation between the MC with and without AL, demonstrating that AI may standardize the evaluation of this anatomical variation and aid surgical planning of implant placement in the mental region.

More under-segmentation in the posterior section of the MC was seen compared to the middle and anterior sections. To evaluate the segmentation of the MC, Agbaje et al.²⁴ also divided the MC into three regions: mental, body, and angle. They observed more under-segmentation of the MC in the angle region than in the body

Mandibular canals	AI segmentation metrics					
	IoU	DSC	Precision	Recall	Accuracy	HDmm95
Anterior loop	0.659 (0.076)	0.792 (0.053)	0.677 (0.075)	0.961 (0.035)	0.998 (0.001)	0.428 (0.102)
Control	0.654 (0.057)	0.789 (0.044)	0.668 (0.061)	0.970 (0.026)	0.997 (0.001)	0.429 (0.039)

Table 1. Mean (standard deviation) of the AI segmentation metrics of the mandibular canals with and without anterior loop (control). $p > 0.05$.

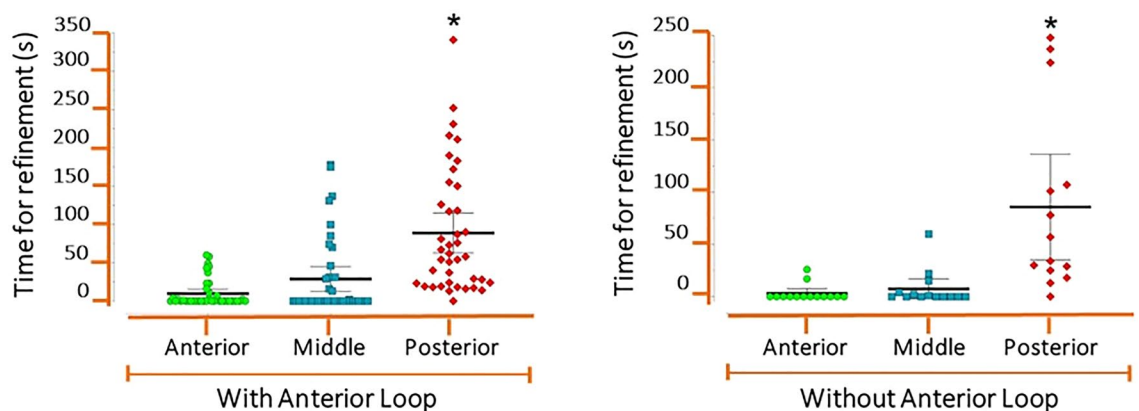


Figure 1. Refined AI segmentation time for the three sections. Each point represents a value. Bars = median, Swiss = interquartile deviation. *Significantly different than other sections.

region; besides, the mental region presented a smaller thickness than the other regions²⁴. These results indicate that the posterior section is the more challenging region to correctly segment the MC. The 3D U-Net network is based on localization and sparse annotation slices. This network allows good results with little training since data augmentation is applied to learn image invariance, which is a challenge for AI^{25,26}. However, as the posterior section presents high variability of position and morphology, especially close to the mandibular foramen^{27,28}, the difference found between the sections in our study may be related to this higher variability in the posterior section. On the other hand, causes of IAN injury are local anesthetic injections, endodontics, ablative surgery, trauma, orthognathic surgery, third molar surgery, and, especially, implant surgery²⁹, most of them related to the anterior and middle sections, where are located the mandibular teeth. Thus, the anterior and middle sections of the MC are the most relevant sections to be correctly segmented and, consequently, avoid nerve injury.

In the present study, AI validation metrics achieved a mean recall value of 0.965, showing the almost perfect specificity of the AI network. It implies that there is little over-segmentation. Conversely, the mean precision value was 0.672, explained by the under-segmentation in the posterior section, which decreased the IoU values. Despite that, accuracy values showed an overall almost perfect segmentation. As the accuracy metrics are calculated based on the entire MC segmentation and sections, if the posterior section, which is less relevant, were not segmented and, thus, not considered in the calculation, our metrics would be even higher.

Lahoud et al.²¹ observed that the algorithm performed better in CBCTs with a higher cortication degree²¹. Since the visibility of the MC may change according to the resolution of the CBCT acquisition protocol³⁰, in the present study, different CBCT machines and resolution protocols were used. Different resolution protocols increased the generalizability of the presently validated tool, achieving a global accuracy of 0.997 for both MC with and without AL. Furthermore, it indicates that our AI-driven tool allows good segmentation, regardless of the cortication of the MC. Thus, it can significantly contribute to help clinicians to correctly detect the MC in complex cases where is more challenging to distinguish it from the trabecular bone.

In the future, we will strive to obtain more generalizability of the cloud-based AI tool by training more CBCT scans from different machines and more patients with anatomical variations and variable dental status, such as pathological jaw lesions in contact with the MC. It would then allow the cloud-based AI tool to predict the performance of the network for all conditions and applications, such as for presurgical planning.

From the present validation study, the AI-driven tool provided accurate segmentation of the mandibular canal, even in the presence of anatomical variations such as an anterior loop. The presently validated dedicated AI tool may aid clinicians to automate the segmentation of neurovascular canals and their anatomical variations. This tool may help surgeons during surgical planning, such as implant placement, especially in the interforaminal region.

Methods

The study was approved by the Ethical Committee Research UZ/KU Leuven (protocol S66447) and performed following the Declaration of Helsinki. In addition, informed consent was obtained from all participants. Lahoud et al.²¹ previously trained and validated the current AI network, as follows²¹.

AI network development. CBCT scans were randomly collected from the local database. The CBCT scans were from dentate patients (mean age 25 ± 11 years old) that acquired the images for oral surgical purposes. The CBCT devices used to acquire the scans were NewTom VGI EVO (QR Verona, Cefla, Verona, Italy), ProMax 3D MAX (Planmeca, Helsinki, Finland), Accuitomo 170 (Morita, Kyoto, Japan), and Scanora 3Dx (Soredex, Tuusula, Finland). In addition, to increase the robustness of the AI network, CBCT scans varying field of view (FOV) dimensions (8×8 to 23×26 cm), voxel sizes (125 to 400 μm), presence of artifacts, spatial resolution, and degrees of MC cortication were selected.

For initially training the AI network, 40 CBCT scans were imported into Romexis software version 5.2.1.R (Planmeca, Helsinki, Finland) for tracing the MC using the built-in tool for nerve annotation. This initial training allowed the development of an initial version of a DL network capable of performing accurate voxel-wise MC segmentation, denoted as Virtual Patient Creator (Relu BV, Leuven, Belgium), which serves as a cloud-based AI tool. Then, 126 new CBCT scans were imported into this DL network to segment of the MC limits on cross-sectional slices by two oral radiologists. Afterward, these segmentations were doubled checked and used to train, refine, and robust the DL network. In addition, data augmentation strategies were applied to artificially increase the dataset and improve the generalizability and robustness of the model²¹.

The architecture to develop the MC segmentation output was based on multiple 3D U-Net networks, an encoder-decoder fully convolutional networks (FCN) with skip connections, applied in medical segmentation problems. The applied FCNs had two paths to allow better performance in classification and high-resolution segmentation of large images^{21,26}. In the contracting path, the images were downsampled through convolutions, rectified linear unit (ReLU), and max pooling operations. Aiding to keep the border pixels lost in every convolution, skip connections propagated the context information to the symmetrical counterparts in the expansive path. Then, in the present study, the first path (encoder) performed a rough segmentation of the MC. The second path (decoder) refined the rough segmentation provided for the first path, producing a full-resolution MC segmentation. For this, the encoder extracted the features from the input image, creating a feature map with global information about the image. The decoder generated a dense segmentation mask of the input. Subsequently, skip connections were applied to combine the feature maps from the encoder to the decoder and improve the localization of the network. Then, a semantic segmentation combined the feature maps from all the layers of the decoder into one single output²⁶ (Fig. 2).

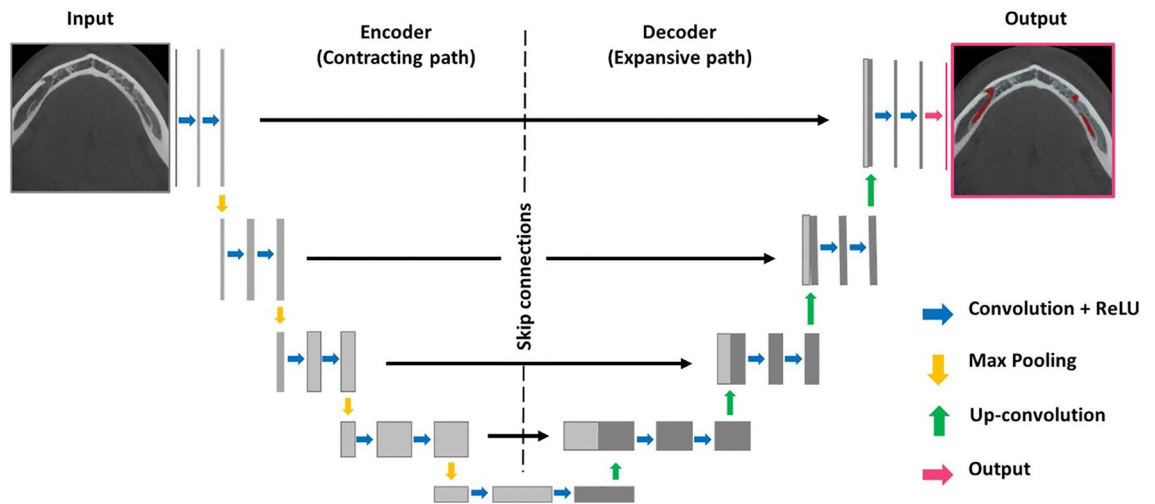


Figure 2. Representation of the 3D U-Net architecture. Adapted from Ronneberger et al.²⁶.

AI network optimization. For AI network optimization to detect AL, 93 new CBCT scans from the UZ Leuven Hospital M3BE database³¹ were collected for further network training, including 30 MC with AL. Therefore, a total of 219 CBCT scans were used for training of the network. The CBCT scans selected for the AI network optimization were from three different CBCT devices NewTom VGI EVO (QR Verona, Cefla, Verona, Italy), ProMax 3D MAX (Planmeca, Helsinki, Finland), and Accuitomo 170 (Morita, Kyoto, Japan), and they were acquired varying FOV dimensions (10×10 , 12×8 , and 15×12 cm), voxel sizes (160, 200, and 250 μm), mA (3–8), and kV (90 and 110). Besides this and to increase the robustness of the network, CBCT scans used in this step were from completely dentate or edentulous zone patients (age between 20–51 years old), varying the presence of artifacts and degrees of mandibular canal cortication, which could be fully corticated, partially corticated, or non-corticated. In addition, CBCT scans showing a FOV that not included both left and right MC and CBCT scans with movement artifacts that duplicated the MC path, were excluded from the sample.

The presence of AL was established as described by Krishnan et al.³. It carried out assessing the horizontal distance between the tangent lines to the most anterior part of the loop and those to the anterior border of the mental foramen³. One radiologist measured this distance in a sagittal view oriented according to the mandible body. This measure was re-evaluated by another radiologist with more than five years of experience. Only cases of AL with ≥ 1 mm (Fig. 3) were considered³. AI generated MC segmentation of the cases (Fig. 4). Then two experts in oral radiology performed expert consensus segmentation, and if needed, they jointly adjusted manually the path, shape, and width of the canal as well as over- and underestimations on cross-sectional slices when deemed necessary (Fig. 5). During training, data augmentation techniques were applied to increase the dataset

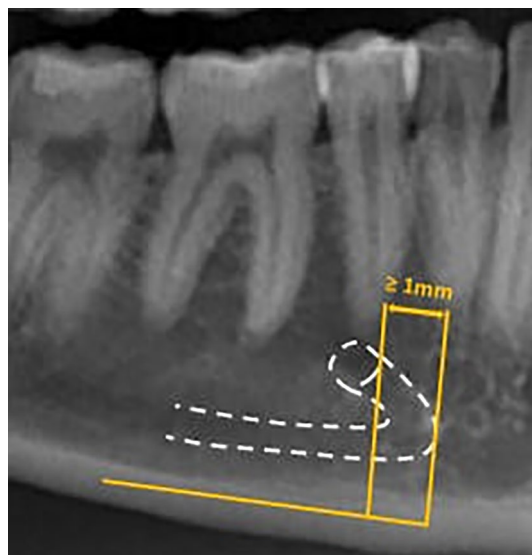


Figure 3. Schematic representation of the measurement of the anterior loop on a reconstructed panoramic image.

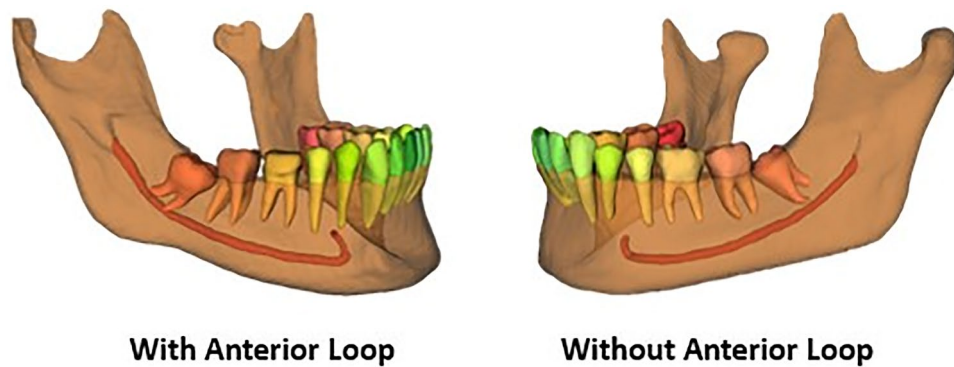


Figure 4. Representation of the segmentation of the mandibular canal with and without an anterior loop.

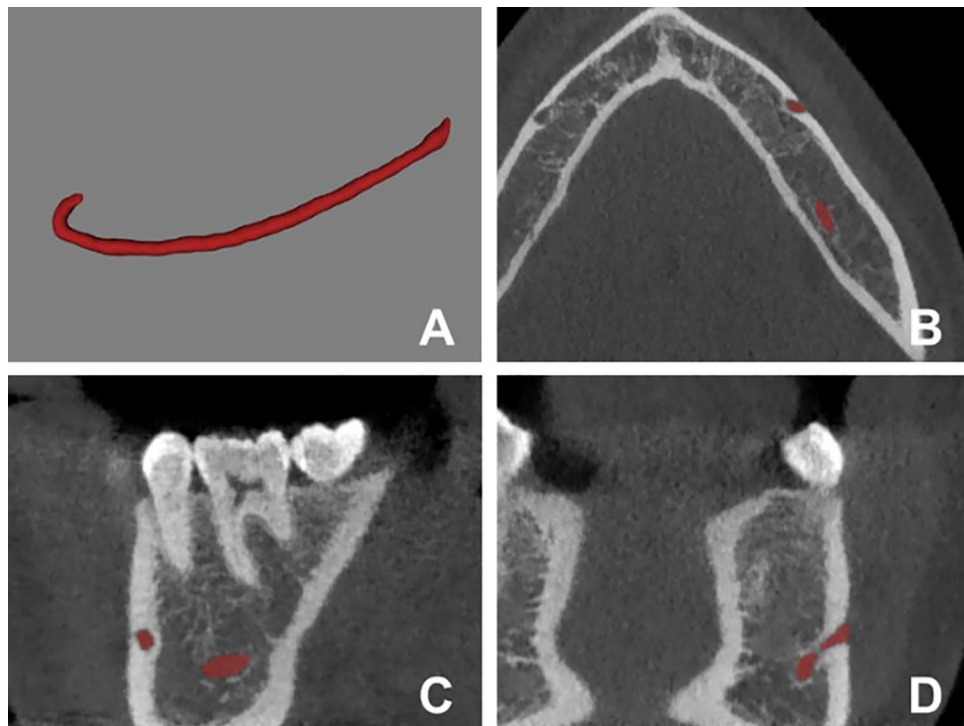


Figure 5. Mandibular canal segmented seen in a 3D view (A), axial view (B), sagittal view (C), and coronal view (D).

artificially. The techniques included random cropping and affine transformations (scaling, rotation, translation, shear, mirroring, and elastic deformations).

Validation and Testing of the AI-optimized network. Subsequently, 27 CBCT scans were used in the validation step to assess the performance of the AI-driven segmentation tool. Then, another 27 CBCT scans were used for the testing step (Fig. 6), in which 40 MC had AL, while 14 had no anatomical variation of the MC (control group). Subsequently, the MC was divided into three sections: anterior (region of premolars and first molar), middle (region of second and third molars), and posterior (posterior region to the third molar until the mandibular foramen) (Fig. 7). Then, the time to adjust AI-driven segmentation was recorded for each section, primarily to allow a secondary analysis for the anterior section, that is crucial for surgery in the canine and premolar area, especially in the presence of AL. Furthermore, correct detection of the middle section is essential, e.g. for implant placement and third molar removal. Finally, the posterior section and the complete neurovascular canal segmentation are crucial for orthognathic surgery, trauma, and other maxillofacial surgical procedures.

The time spent to segment the MC automatically and to perform expert refinements of AI-driven over- and under-segmentation was recorded in each section. Segmentation of the AI-driven tool and its refinements were exported as Standard Tessellation Language files. The refined AI segmentation was considered the ground truth. Then voxel-level annotations were used to calculate the values of true positive (TP), false positive (FP), true

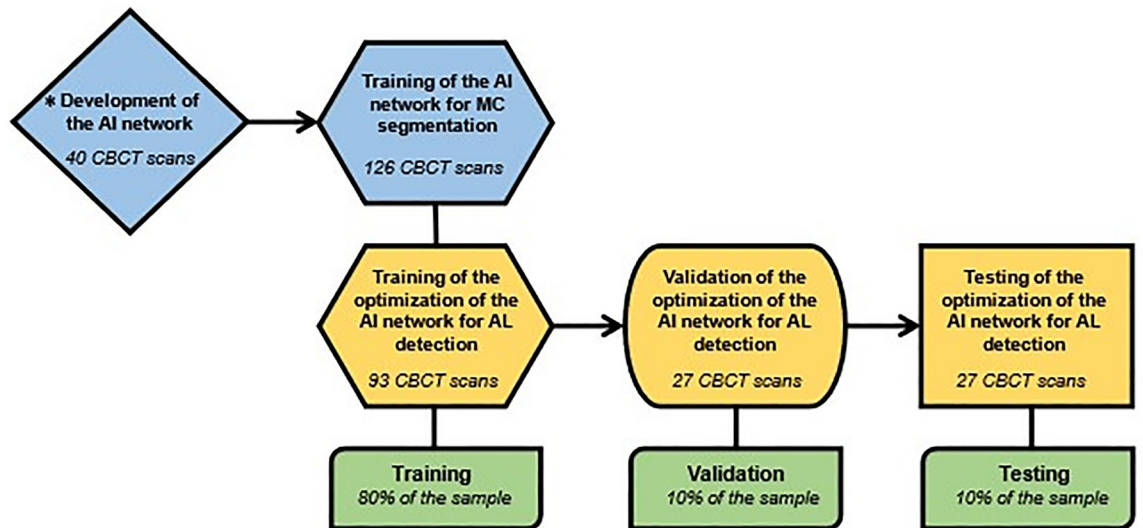


Figure 6. Flowchart of the sample distribution during the training, validation, and testing of the AI network. Blue forms were performed by Lahoud et al.²¹, while the yellow steps were performed in the present study.

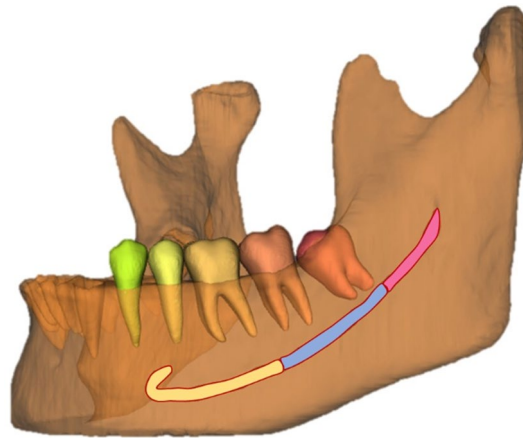


Figure 7. Mandibular canal divided into three sections: anterior (yellow), middle (blue), and posterior (pink).

negative (TN), and false negative (FN) regarding the number of pixels that the method predicted, as described below.

- TP: Voxels segmented by AI and segmented by the ground truth.
- FP: Voxels segmented by AI and non-segmented by the ground truth.
- TN: Voxels non-segmented by AI and non-segmented by the ground truth.
- FN: Voxels non-segmented by AI and segmented by the ground truth.

These values were applied to calculate the accuracy metrics for comparison of AI-driven and refined AI segmentation.

The following accuracy metrics were calculated:

- Intersection over union (IoU): Represents the similarity between the predicted object and the ground truth counterpart (area of overlap between expert and AI-driven segmentation that voxels match exactly). An IoU of 1 is a perfect segmentation³². It is defined by the equation:

$$IoU = \frac{TP}{FP + TP + FN}$$

- Dice Similarity Coefficient (DSC): Amount of intersection between the AI-driven segmentation and the ground truth³³, being a DSC of 1 considered as a perfect segmentation, defined by the equation:

$$DSC = \frac{2 \times TP}{(TP + FP) + (TP + FN)}$$

- 95% Hausdorff Distance (HD_{mm95}): Indicates the 95th percentile of the largest segmentation error measuring the longest distance between a point in the ground truth (A) and its closest point in the AI-driven segmentation (B) measured in millimeters³⁴. An HD_{mm95} of 0 is a perfect segmentation. Its equation is:

$$95HD(A, B) = \text{percentile}[h(A, B) \cup h(B, A), 95th]$$

$$h(A, B) = \max_{a \in A} \min_{b \in B} \|a - b\|$$

$$h(B, A) = \max_{b \in B} \min_{a \in A} \|b - a\|$$

- Precision: Based on region overlapping, measure the matching direction between the expert manual segmentation and the AI-driven segmentation, being the manual segmentation used as reference and 1 considered as a perfect segmentation³⁵, defined by the following equation:

$$\text{Precision} = \frac{TP}{TP + FP}$$

- Recall: Similar to the precision measure but using the AI-driven segmentation as reference. The Precision and Recall measure the agreement between the oriented boundary edge elements of the two segmentations³⁵. A recall of 1 is considered a perfect segmentation. The recall equation is defined as:

$$\text{Recall} = \frac{TP}{TP + FN}$$

- Accuracy: Weighted arithmetic mean that can be expressed both as weighted mean average of Precision and Inverse Precision and as weighted mean average of Recall and Inverse Recall²¹, with 1 being considered as perfect segmentation, defined by:

$$\text{Accuracy} = \frac{TP + TN}{TP + TN + FP + FN}$$

Finally, the statistical analysis was performed using the GraphPad software (GraphPad Software, Inc., San Diego, CA, USA). The Mann–Whitney test was used to compare the accuracy metrics between the MC with and without AL. The Kruskal Wallis test compared the time of refinement between the MC with and without AL and between the MC sections ($\alpha = 5\%$).

Data availability

The datasets used and/or analyzed during the current study are available from the corresponding author upon reasonable request.

Received: 2 March 2023; Accepted: 28 June 2023

Published online: 04 July 2023

References

1. Jacobs, R. *et al.* Neurovascularization of the anterior jaw bones revisited using high-resolution magnetic resonance imaging. *Oral Surg. Oral Med. Oral Pathol. Oral Radiol. Endodontol.* **103**, 683–693 (2007).
2. Jeon, Y. H. *et al.* 3-Dimensional reconstruction of mandibular canal at the interforaminal region using micro-computed tomography in Korean. *J. Adv. Prosthodont.* **9**, 470 (2017).
3. Krishnan, U., Monsour, P., Thaha, K., Laloo, R. & Moule, A. A limited field cone-beam computed tomography–based evaluation of the mental foramen, accessory mental foramina, anterior loop, lateral lingual foramen, and lateral lingual canal. *J. Endod.* **44**, 946–951 (2018).
4. Bou Serhal, C., Jacobs, R., Flygare, L., Quiryren, M. & Van Steenberghe, D. Perioperative validation of localisation of the mental foramen. *Dentomaxillofac. Radiol.* **31**, 39–43 (2002).
5. Gupta, A. *et al.* Assessment of anterior loop of inferior alveolar nerve and its anatomic variations with age, gender, and dentition status in Indian population: A CBCT study. *Int. J. Dent.* **2021**, 66 (2021).
6. de Oliveira-Santos, C. *et al.* Assessment of variations of the mandibular canal through cone beam computed tomography. *Clin. Oral Investig.* **16**, 387–393 (2012).
7. Mraiwa, N., Jacobs, R., Van Steenberghe, D. & Quiryren, M. Clinical assessment and surgical implications of anatomic challenges in the anterior mandible. *Clin. Implant Dent. Relat. Res.* **5**, 219–225 (2003).
8. Bornstein, M., Scarfe, W., Vaughn, V. & Jacobs, R. Cone beam computed tomography in implant dentistry: A systematic review focusing on guidelines, indications, and radiation dose risks. *Int. J. Oral Maxillofac. Implants* **29**, 55–77 (2014).
9. Wei, X., Gu, P., Hao, Y. & Wang, J. Detection and characterization of anterior loop, accessory mental foramen, and lateral lingual foramen by using cone beam computed tomography. *J. Prosthet. Dent.* **124**, 365–371 (2020).
10. Wong, S. K. & Patil, P. G. Measuring anterior loop length of the inferior alveolar nerve to estimate safe zone in implant planning: A CBCT study in a Malaysian population. *J. Prosthet. Dent.* **120**, 210–213 (2018).
11. Jacobs, R., Quiryren, M. & Bornstein, M. M. Neurovascular disturbances after implant surgery. *Periodontology* **2000**(66), 188–202 (2014).
12. Mishra, S. K., Nahar, R., Gaddale, R. & Chowdhary, R. Identification of anterior loop in different populations to avoid nerve injury during surgical procedures—A systematic review and meta-analysis. *Oral Maxillofac. Surg.* **25**, 159–174 (2021).
13. de Brito, A. C. R., Nejaïm, Y., Freitas, D. Q. & de Oliveira Santos, C. Panoramic radiographs underestimate extensions of the anterior loop and mandibular incisive canal. *Imaging Sci. Dent.* **46**, 159 (2016).

14. Chen, Z., Chen, D., Tang, L. & Wang, F. Relationship between the position of the mental foramen and the anterior loop of the inferior alveolar nerve as determined by cone beam computed tomography combined with mimics. *J. Comput. Assist. Tomogr.* **39**, 86–93 (2015).
15. Juodzbalys, G., Wang, H.-L. & Sabalys, G. Anatomy of mandibular vital structures. Part II: Mandibular incisive canal, mental foramen and associated neurovascular bundles in relation with dental implantology. *J. Oral Maxillofac. Res.* **1**, 66 (2010).
16. Hung, K., Montalvao, C., Tanaka, R., Kawai, T. & Bornstein, M. M. The use and performance of artificial intelligence applications in dental and maxillofacial radiology: A systematic review. *Dentomaxillofac. Radiol.* **49**, 66 (2019).
17. Khanagar, S. B. *et al.* Developments, application, and performance of artificial intelligence in dentistry—A systematic review. *J. Dent. Sci.* **16**, 508–522 (2021).
18. Leite, A. F., Vasconcelos, K. de F., Willems, H. & Jacobs, R. Radiomics and machine learning in oral healthcare. *PROTEOMICS Clin. Appl.* **14**, 1900040 (2020).
19. Jaskari, J. *et al.* Deep learning method for mandibular canal segmentation in dental cone beam computed tomography volumes. *Sci. Rep.* **10**, 5842 (2020).
20. Kwak, G. H. *et al.* Automatic mandibular canal detection using a deep convolutional neural network. *Sci. Rep.* **10**, 5711 (2020).
21. Lahoud, P. *et al.* Development and validation of a novel artificial intelligence driven tool for accurate mandibular canal segmentation on CBCT. *J. Dent.* **116**, 103891 (2022).
22. Filo, K., Schneider, T., Locher, M. C., Kruse, A. L. & Lübbers, H. T. The inferior alveolar nerve's loop at the mental foramen and its implications for surgery. *J. Am. Dent. Assoc.* **145**, 260–269 (2014).
23. Uchida, Y. *et al.* Measurement of anterior loop length for the mandibular canal and diameter of the mandibular incisive canal to avoid nerve damage when installing endosseous implants in the interforaminal region: A second attempt introducing cone beam computed tomography. *J. Oral Maxillofac. Surg.* **67**, 744–750 (2009).
24. Agbaje, J. O. *et al.* Tracking of the inferior alveolar nerve: Its implication in surgical planning. *Clin. Oral Investig.* **21**, 2213–2220 (2017).
25. Çiçek, Ö., Abdulkadir, A., Lienkamp, S. S., Brox, T. & Ronneberger, O. 3D U-Net: Learning Dense Volumetric Segmentation from Sparse Annotation 424–432 (2016). https://doi.org/10.1007/978-3-319-46723-8_49
26. Ronneberger, O., Fischer, P. & Brox, T. U-Net: Convolutional networks for biomedical image segmentation. In *International Conference on Medical Image Computing and Computer-Assisted Intervention MICCAI* 234–241 (Springer, 2015). [arXiv:1505.04597](https://arxiv.org/abs/1505.04597)
27. Zhou, C., Jeon, T.-H., Jun, S.-H. & Kwon, J.-J. Evaluation of mandibular lingula and foramen location using 3-dimensional mandible models reconstructed by cone-beam computed tomography. *Maxillofac. Plast. Reconstr. Surg.* **39**, 30 (2017).
28. Ahn, B.-S. *et al.* Cone-beam computed tomography of mandibular foramen and lingula for mandibular anesthesia. *Imaging Sci. Dent.* **50**, 125 (2020).
29. Renton, T. Oral surgery: Part 4. Minimising and managing nerve injuries and other complications. *Br. Dent. J.* **215**, 393–399 (2013).
30. Zaki, I. M., Hamed, W. M. & Ashmawy, M. S. Effect of CBCT dose reduction on the mandibular canal visibility: Ex vivo comparative study. *Oral Radiol.* **37**, 282–289 (2021).
31. Vranckx, M. *et al.* Do anatomical variations of the mandibular canal pose an increased risk of inferior alveolar nerve injury after third molar removal? *Clin. Oral Investig.* <https://doi.org/10.1007/s00784-021-04076-3> (2021).
32. Rezatofghi, H. *et al.* Generalized intersection over union: A metric and a loss for bounding box regression. In *Proceedings of the IEEE Computing Society Conference on Computer Vision and Pattern Recognition* 2019–June 658–666 (2019).
33. Popovic, A., de la Fuente, M., Engelhardt, M. & Radermacher, K. Statistical validation metric for accuracy assessment in medical image segmentation. *Int. J. Comput. Assist. Radiol. Surg.* **2**, 169–181 (2007).
34. Liu, Z. *et al.* Automatic segmentation of clinical target volumes for post-modified radical mastectomy radiotherapy using convolutional neural networks. *Front. Oncol.* **10**, 1–8 (2021).
35. Zhang, X., Feng, X., Xiao, P., He, G. & Zhu, L. Segmentation quality evaluation using region-based precision and recall measures for remote sensing images. *ISPRS J. Photogramm. Remote Sens.* **102**, 73–84 (2015).

Acknowledgements

This study was financed in part by the Coordenação de Aperfeiçoamento de Pessoal de Nível Superior — Brasil (CAPES) — Finance Code 001.

Author contributions

R.J. conceived the ideas; N.O.S and F.F.P. designed the study; N.O.S. and L.N. collected the data; N.O.S., F.F.P., P.L., and F.C.G. contributed data; N.O.S. drafted the paper; R.J. and F.C.G. revised it. All authors have read and approved the final manuscript.

Funding

Open access funding provided by Karolinska Institute.

Competing interests

The authors declare no competing interests.

Additional information

Correspondence and requests for materials should be addressed to R.J.

Reprints and permissions information is available at www.nature.com/reprints.

Publisher's note Springer Nature remains neutral with regard to jurisdictional claims in published maps and institutional affiliations.



Open Access This article is licensed under a Creative Commons Attribution 4.0 International License, which permits use, sharing, adaptation, distribution and reproduction in any medium or format, as long as you give appropriate credit to the original author(s) and the source, provide a link to the Creative Commons licence, and indicate if changes were made. The images or other third party material in this article are included in the article's Creative Commons licence, unless indicated otherwise in a credit line to the material. If material is not included in the article's Creative Commons licence and your intended use is not permitted by statutory regulation or exceeds the permitted use, you will need to obtain permission directly from the copyright holder. To view a copy of this licence, visit <http://creativecommons.org/licenses/by/4.0/>.

© The Author(s) 2023